OPEN

Ubiquinone-quantum dot bioconjugates for *in vitro* and intracellular complex I sensing

Wei Ma[1]*, Li-Xia Qin[1]*, Feng-Tao Liu[2], Zhen Gu[1], Jian Wang[2], Zhi Gang Pan[3], Tony D. James[4] & Yi-Tao Long[1]

[1]State Key Laboratory of Bioreactor Engineering & Department of Chemistry, East China University of Science and Technology, 130 Meilong Road, Shanghai, 200237, P. R. China, [2]Department of Neurology, Huashan Hospital Affiliated to Fudan University, 12 Wulumuqi Zhong Road, Shanghai, 200040, P. R. China, [3]Department of Medicine, Zhongshan Hospital Affiliated to Fudan University, 180 Fenglin Road, Shanghai, 200032, P. R. China, [4]Department of Chemistry, University of Bath, Claverton Down, Bath, BA2 7AY, UK.

Quantum dots (QDs) have attracted increasing interest in bioimaging and sensing. Here, we report a biosensor of complex I using ubiquinone-terminated disulphides with different alkyl spacers (Q_nNS, n = 2, 5 and 10) as surface-capping ligands to functionalise CdSe/ZnS QDs. The enhancement or quenching of the QD bioconjugates fluorescence changes as a function of the redox state of Q_nNS, since QDs are highly sensitive to the electron-transfer processes. The bioconjugated Q_nNS-QDs emission could be modulated by complex I in the presence of NADH, which simulates an electron-transfer system part of the mitochondrial respiratory chain, providing an *in vitro* and intracellular complex I sensor. Epidemiological studies suggest that Parkinson's patients have the impaired activity of complex I in the electron-transfer chain of mitochondria. We have demonstrated that the Q_nNS-QDs system could aid in early stage Parkinson's disease diagnosis and progression monitoring by following different complex I levels in SH-SY5Y cells.

Parkinson's disease (PD) is a complex neurodegenerative disorder affecting the elderly with many different causes but probably then evolves *via* common pathways[1,2]. Currently, diagnosis of PD almost relies on clinical acumen. There are no established laboratory tests or biosensors that can reliably and specifically identify PD. Moreover, differential diagnosis for PD can be rather challenging due to overlapping symptoms, particularly in its early stages[3–5]. Thus, there is an urgent clinical need to develop biosensors for the diagnosis of PD and differentiation of disease progression. Current evidence suggests that mitochondrial NADH:ubiquinone oxidoreductase (complex I) inhibition may be the central cause of sporadic PD and that disorders in complex I causes the demise of dopamine neurons, which contributes to the major clinical symptoms of PD[6–8]. The relationship between loss of complex I activity and PD progression may provide a path to early diagnosis and monitoring of PD.

Complex I is the first enzyme of the mitochondrial respiratory chain and plays a central role in cellular energy production, coupling electron-transfer between NADH and ubiquinone to proton translocation, helping to provide the proton-motive force required for the synthesis of adenosine triphosphate[9]. As an essential cofactor in the respiratory chain, ubiquinone, also known as coenzyme Q, is found at the hydrophobic core of the phospholipid bilayer of the inner membrane of mitochondria[10] and serves as a mobile carrier transferring electrons and protons[11,12]. The activities of reversible redox cycling between the ubiquinone and ubiquinol in the electron transport chain allow the ubiquinone molecule to function as a valuable mediator.

Semiconductor quantum dots (QDs) have widespread applicability in areas ranging from *in vivo* imaging[13,14] and clinical diagnostics[15,16] in biomedicine to environmental monitoring for public health and security due to their unique optical properties, including tunable fluorescence narrow emission, broad absorption profiles, high signal brightness and superior photostability[17,18]. In addition, QDs are extremely sensitive to the presence of additional charges either on their surfaces or in the surrounding environment, which can lead to a variety of optical properties and electronic consequences[13]. The redox potential of capping molecules can be chosen to maximize the efficiency of charge transfer to promote transfer of external electrons and holes to either the QDs' core conduction band (CB) or the QDs' surface states[15]. Thus, controlling charge transport across redox-active molecules functionalised QDs has generated interest for advanced molecular and cellular imaging as well as

ultrasensitive biosensing[14,19]. For instance, QD-dopamine bioconjugates stain dopamine-receptor-expressing cells in redox-sensitive patterns[20]. Dopamine as an electron donor could sensitize QDs through different mechanisms involving reactive oxygen species (ROS)[20–23]. Recently, we demonstrated that coupling QDs with cytochrome c is capable of fluorescence imaging of a superoxide radical with high specificity[24]. Ubiquinone-coupled QDs could be used for quantitative detection of ROS in living cells[25]. Cumulatively, these results confirm a role for redox molecules, and especially quinone, in charge-transfer interactions with QDs; however, the improvement of QD bioconjugates compatibility in biological system and how to exploit it as biosensors for clinical diagnostic applications is lacking.

Herein, we report the design and preparation of colloidal CdSe/ZnS QDs utilizing three ubiquinone-terminated disulphides with different alkyl spacer, Q_nNS (n=2, 5 and 10), appended with 1,2,3-triazole that are synthesized as surface-capping ligands to functionalise QDs (Q_nNS-QDs). Using the Q_nNS-QD bioconjugates, we found that either quenching or enhancing the QDs' emission is reversibly tuned by the redox state of surface-capping layer, following the transformation between oxidized ubiquinone (Q_nNS) and reduced ubiquinol (HQ_nNS). There is a direct interplay between ubiquinone and NADH in the enzymatic reaction of the electron transport chain and it enables us to follow the activities of complex I to develop a unique optical sensor for complex I. We have demonstrated that the emission of Q_nNS-QDs is enhanced with complex I in the presence of NADH, which is attributed to the oxidized ubiquinone being reduced to ubiquinol on the QD surface. Our strategy is aimed at using the QD bioconjugates to follow deficient levels of complex I in human neuroblastoma SH-SY5Y cells. We believe our approach may hold particular promise as a powerful fluorescence biosensor targeting the clinical diagnosis of PD.

Results

Design of surface-capping Q_nNS ligands. We designed QD bioconjugates for biosensing complex I using ubiquinone-terminated disulphide ligands and 550-nm-emitting core-shell CdSe/ZnS QDs. Three ligands Q_2NS, Q_5NS and $Q_{10}NS$ were prepared using a facile click reaction using copper(I) tris(benzyltriazolylmethyl) amine-catalysed 1,2,3-triazole formation[26] between alkylazide-disulphides and ubiquinone with terminal alkynes (Fig. 1a). We introduced the quinoid moiety in the Q_nNS ligands to achieve the redox-switchable fluorescence properties that could be useful for signal multiplexing. The 1,2,3-triazole groups, similar to histidine[27], could enhance the compatibility of Q_nNS-QDs in biological systems. Three alkyl linkers confer different abilities of electron-transfer to either the QDs' core or the surface of QDs. Finally, the disulfide group facilitates binding of Q_nNS to the QDs. The synthetic procedures and structural characterisation of the Q_nNS ligands are presented in the Supplementary Information.

Fluorescence spectra of Q_nNS and HQ_nNS-functionalised CdSe/ZnS QDs. We investigated the fluorescence effects of QD bioconjugates by using QDs capped with oxidized Q_nNS and reduced HQ_nNS because QDs are prone to exchange electrons or energy with the attached ligands upon excitation, resulting in their fluorescence change. As shown in Figure 2a–c, for Q_nNS-QD bioconjugates, the fluorescence intensity gradually decreased with increasing ratios (20–100) of Q_nNS to QDs compared to the unconjugated QDs, at high Q_nNS (ratio 120) levels quenching of the QD bioconjugates was saturated giving an average coverage of 100 Q_nNS molecules per CdSe/ZnS QDs. As can be seen, fluorescence quenching efficiency was dependent on the alkyl chain spacer of Q_nNS, since a more pronounced quenching was observed for the shorter Q_2NS-modified QDs. As spacer length increases, the quenching efficiency of the three ubiquinone-functionalised CdSe/ZnS QDs (ratio 100) decreases: ~77% (Q_2NS-QDs), ~56% (Q_5NS-QDs) and ~37%

($Q_{10}NS$-QDs), respectively. We further examined fluorescence effects of the QDs modified with the reduced ubiquinol, HQ_nNS. Surprisingly, the fluorescence intensity of reduced HQ_nNS-QD bioconjugates gradually enhanced at given ratio of HQ_nNS to QDs from 20 to 100. At a HQ_nNS/QDs ratio of 120, no additional increase of fluorescence was observed which indicated that on average 100 HQ_nNS ligands assembled to these CdSe/ZnS QDs (Fig. 2a–c). The alkyl chain spacer-dependent trend for fluorescence enhancement of HQ_nNS-QDs (ratio 100) was ~44% (HQ_2NS-QDs), ~33% (HQ_5NS-QDs) and ~23% ($HQ_{10}NS$-QDs), respectively. The insets in Figure 2a–c schematically depict the linear correspondence of QD bioconjugates fluorescence changes as a function of either ubiquinol or ubiquinone ratio and reaches saturation.

Electrochemical switching fluorescence of Q_nNS modified CdSe/ZnS QDs. In this work, we investigated the redox properties of the surface-capping ligands effect on the fluorescence of QD bioconjugates following the transformation between Q_nNS and HQ_nNS state when applying constant potential. As depicted in Figure 3a, b and c, at the applied reduction potential of −0.30 V vs. SCE, the fluorescence intensity of Q_2NS, Q_5NS and $Q_{10}NS$-modified CdSe/ZnS QDs increased during electrolysis. It should be noted that the Q_nNS ligands are reduced to generate the ubiquinol, which resulted in an enhancement of QDs' fluorescence. When applying a constant potential of 0.10 V vs. SCE to Q_2NS-QDs (50 s), Q_5NS-QDs (55 s) and $Q_{10}NS$-QDs (60 s), a decrease in fluorescence intensity was observed indicating that the capping layer of HQ_nNS was reoxidized to the Q_nNS layer. We then looked to confirming that the redox couple ubiquinon/ubiquinol is responsible for the QDs' fluorescence quenching/enhancement. Control experiments indicated that no effect was observed on the fluorescence intensity when unmodified CdSe/ZnS QDs were used at a potential of −0.30 V or 0.10 V vs. SCE under the same conditions (data not shown). Moreover, in situ UV-vis spectroelectrochemical experiments have also confirmed that transformation of surface-capping layer between ubiquinone and ubiquinol could be modulated effectively by electrochemistry (see Fig. S1, Supplementary Information).

Figure 3d, e and f present the time-dependent changes in fluorescence intensity for ubiquinone/ubiquinol upon repeated reduction and oxidation cycles of the Q_nNS-QDs with applied potential. Clearly, the fluorescence intensity of Q_2NS, Q_5NS and $Q_{10}NS$-modified QDs are enhanced significantly with an increase of electrolysis time (0~50 s, 0~55 s and 0~60 s, respectively) at the potential of −0.30 V vs. SCE. Subsequently, QDs' fluorescence intensity gradually decreased at the potential of 0.10 V vs. SCE with electrolysis time (0~50 s, 0~55 s and 0~60 s, respectively). Clearly demonstrating that the oxidized capping layer (ubiquinone) converts to its reduced form (ubiquinol) and is reoxidized again (ubiquinone) on the QD surface. These results show excellent reversibility over three cycles with only small losses of fluorescence intensity in the subsequent cycles and rapid transformation between redox states of surface-capping ligand, Q_nNS and HQ_nNS, circa 2 min. Overall, these results indicate the feasibility of using such QD bioconjugates as switchable fluorescence sensors.

The biocatalytic reduction of Q_nNS-modified CdSe/ZnS QDs utilizing complex I and NADH. To further investigate the viability of Q_nNS-CdSe/ZnS QDs' compatibility in biological systems, we coupled the biocatalytic reduction to complex I enzymatic reaction using NADH cofactors to mimic the well-known 'Q cycle' model in electron-transfer process of the respiratory chain (Fig. 1b)[28]. As shown in Figure 4a, b, c, the time-dependent fluorescence intensity of Q_nNS-QD bioconjugates increase upon the interaction with complex I (4.9 U) in the presence of 10 mM NADH. The results indicate that the biocatalytic two-electron, two-proton reduction of Q_nNS utilising complex I and NADH cofactor results in HQ_nNS-functionalised QDs and switches on the QDs' fluorescence. The
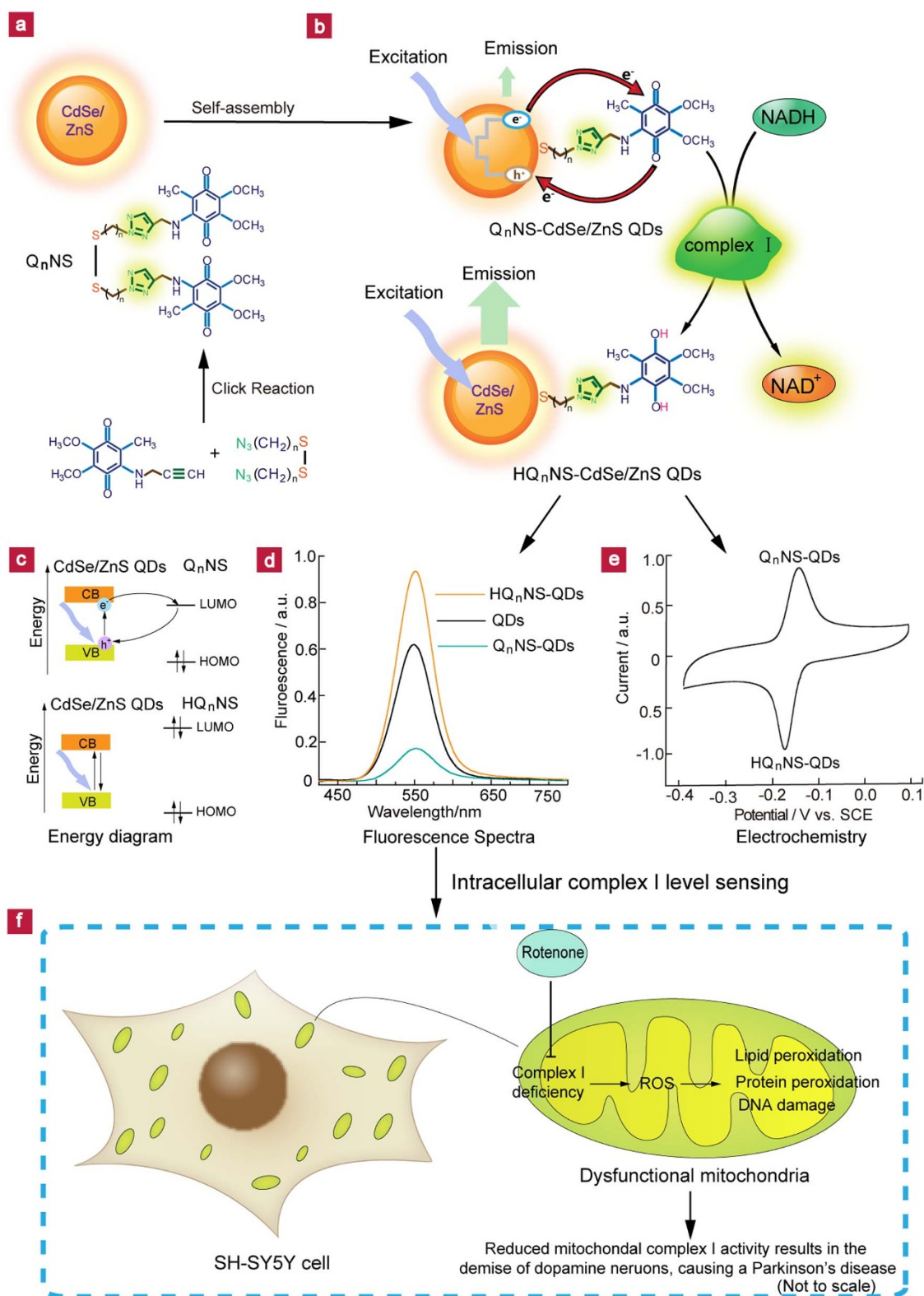
Figure 1 | Schematic of ubiquinone-CdSe/ZnS QDs as redox fluorescence biosensor for Parkinson's disease diagnosis. (a), Ubiquinone-terminated disulphides (**Q$_n$NS**) synthesis and self-assembly of **Q$_n$NS** on to CdSe/ZnS QDs. (b), Conceptual visualisation of **Q$_n$NS**-QDs as complex I sensor *in vitro*. Under oxidized state (**Q$_n$NS**), ubiquinone functions as a favorable electron acceptor, this results in effective QDs' fluorescence quenching. Addition of complex I to **Q$_n$NS**-QDs solution in the presence of NADH, ubiquinone coupled electron transfer and proton translocation from NADH, producing reduced ubiquinol (**HQ$_n$NS**) form on the surface of QDs to mimic the initial stages of the respiratory chain. Ubiquinol when in close proximity to the QDs produces fluorescence enhancement. (c), Energetic diagram of the QDs bioconjugates between QDs and **Q$_n$NS/HQ$_n$NS**. (d), Fluorescence spectra of ubiquinone/ubiquinol- functionalised CdSe/ZnS QDs. (e), Cyclic voltammetry of **Q$_n$NS**-CdSe/ZnS QDs. (f), Visualisation of **Q$_n$NS**-CdSe/ZnS QDs as an intracellular complex I sensor. The mitochondrial-specific neurotoxin, rotenone, inhibits complex I and leads to Parkinson's-like pathogenesis. Parkinson's disease is characterised by impaired activity of complex I in mitochondria.
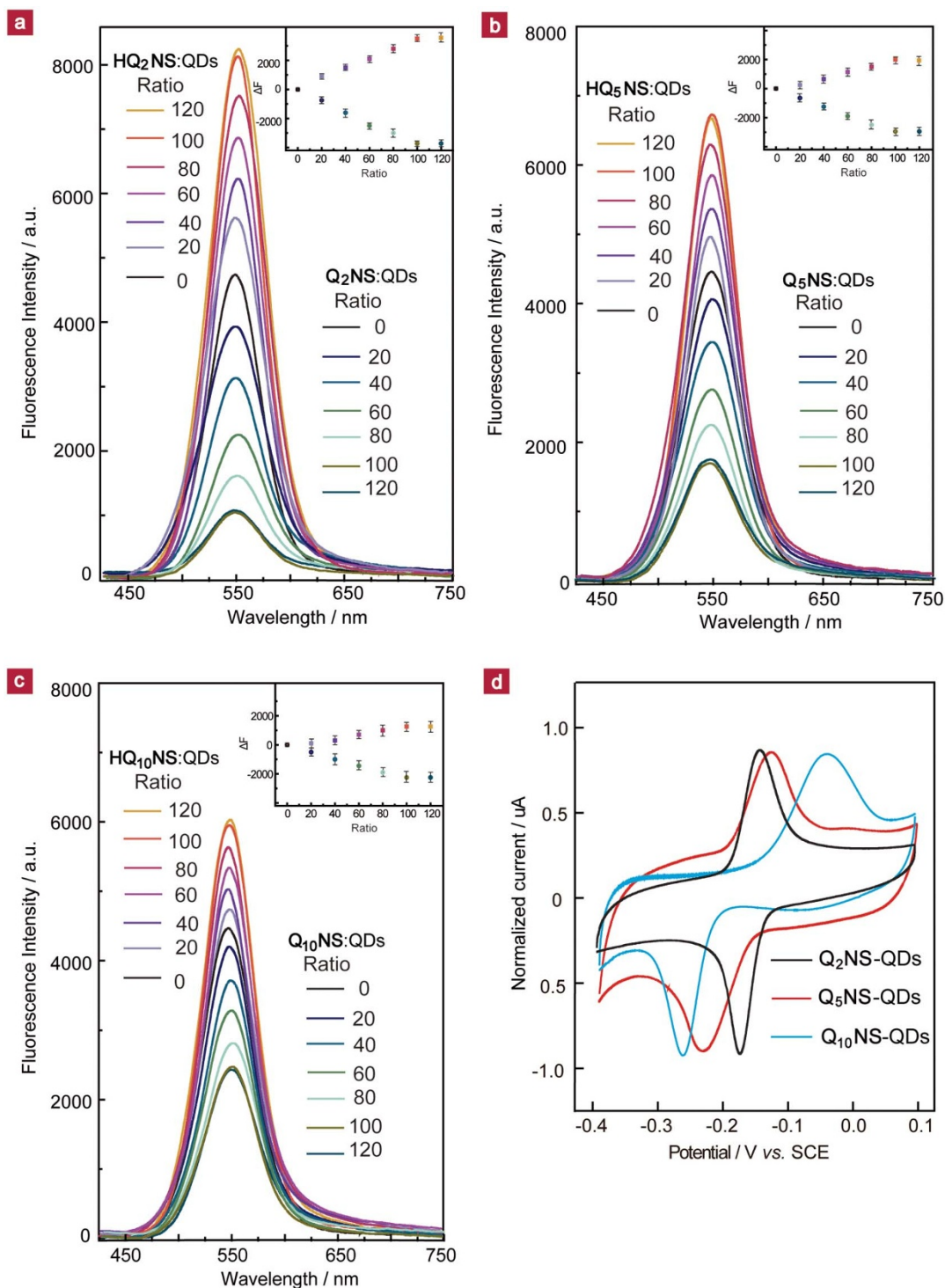
Figure 2 | Effects of ubiquinone and ubiquinol on fluorescence spectra of QDs. (a–c), Representative fluorescence spectra collected from 550-nm-emitting hydrophilic CdSe/ZnS QDs (0.2 M PBS buffer; pH 8.0) recorded before and after self-assembly with an increasing ratio of ubiquinol and ubiquinone added to PBS buffer at Q_2NS (a), Q_5NS (b) and $Q_{10}NS$ (c). Spectra were collected on a Shimadzu Cary Eclipse (Varian) fluorometer with 350 nm excitation. Inset: Plot of QD bioconjugates fluorescence at 550 nm versus HQ_nNS and Q_nNS to QDs ratio. Standard deviations are calculated from at least three replicate samples are shown. (d), Normailized cyclic voltammetry of Q_nNS modified QDs on glassy carbon electrode in PBS buffer of pH = 8.0 at a 100 mV·s^{-1} scan rate. SCE is saturated calomel electrode.

insets in Figure 4a, b, c illustrate that QDs' fluorescence intensity increased as a function of incubation time, and reaches saturation after ~4.5, ~5.0 and ~5.5 min for the Q_2NS, Q_5NS and $Q_{10}NS$-QDs systems, respectively. Notably, we incorporated a 1,2,3-triazole group in these ligands that could be useful for enzyme affinity.

Therefore in control experiments linking groups without triazoles Q_nS (see Fig. S2, Supplementary Information) were prepared. Figure S2 shows similar time-dependent fluorescence enhancements from QDs assembled with Q_nS except a significant increase in incubation time compared to triazole linked Q_nNS-QDs. The fluorescence
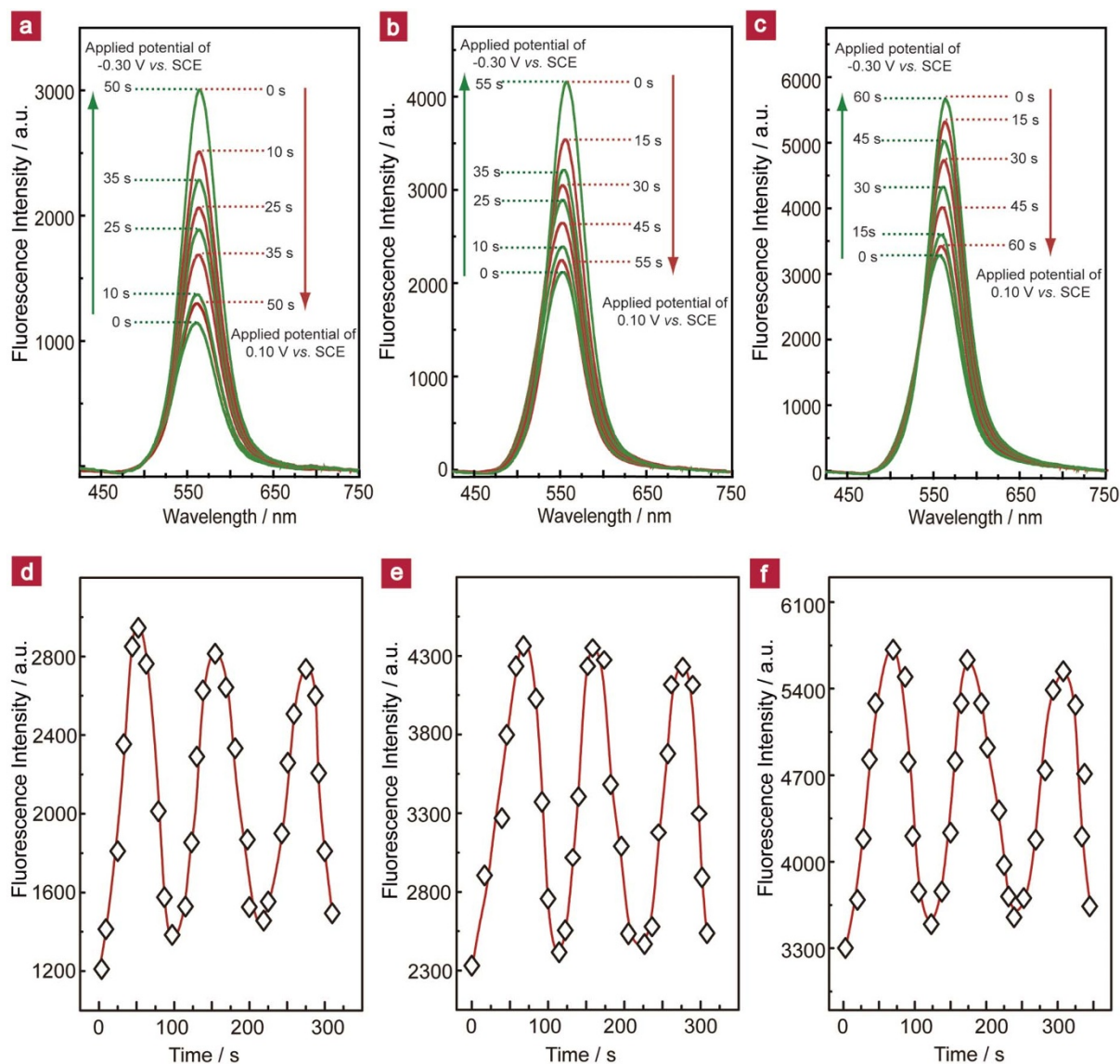
Figure 3 | The fluorescence spectra changes with applied potential. (a–c), The fluorescence emission spectra of Q_2NS (a), Q_5NS (b) and $Q_{10}NS$ (c) functionalised CdSe/ZnS QDs changes with applied potential. At the applied potential of -0.30 V *vs.* SCE, the fluorescence intensity of QD bioconjugates gradually increased. At a constant applied potential of 0.10 V *vs.* SCE, the fluorescence intensity decreased over time. (d–f), Time-dependent fluorescence intensity changes upon the redox cycle of Q_2NS (d), Q_5NS (e) and $Q_{10}NS$ (f) functionalised CdSe/ZnS QDs with applied potential. The fluorescence cyclic change follows with a cyclic change of the electrolysis time.

intensity reaches saturation after $\sim$7.0, $\sim$8.0 and $\sim$10.5 min for Q_1S, Q_5S and $Q_{10}S$-QDs system, respectively. This is because the triazole groups behave similar to the histidine ligand could be used to cap enzyme through proteins or peptides-affinity coordination of triazole residues for simultaneously improving QD bioconjugates' aqueous dispersion and biocompatibility[27]; Which results in the triazole Q_nNS ligands having better binding affinity with complex I.

As shown in Figure 4d, as the concentrations of complex I increase, the fluorescence intensity of Q_nNS-QDs in the presence of NADH becomes more intense with respect to the initial fluorescence intensity (F_0), which agrees with the functionalisation of higher HQ_nNS concentrations on the QDs' surface. However, control experiments revealed that the Q_nNS-QDs' fluorescence was insensitive to high concentrations of complex I when NADH was excluded from the system (data not shown). The changes in the fluorescence intensities of three QD systems were obtained with NADH for complex I in the range of 0.02 U to 4.9 U, 0.03 U to

4.1 U and 0.04 U to 3.1 U for Q_2NS, Q_5NS and $Q_{10}NS$, respectively. The Q_2NS-QDs showed a lower detection limit and wider response range compared to both Q_5NS and $Q_{10}NS$-QDs.

Moreover, the corresponding spectral changes in absorption by UV–vis spectroscopy were monitored upon addition of complex I in the presence of NADH. As shown in Figure 4e, in the absence of complex I, the solution displays a band at 275 nm, attributed to the π-π* absorption spectrum of ubiquinone and NADH. The remaining peak at 340 nm, is characteristic of NADH. Clearly, as the concentration of complex I increases, the absorbance at 275 nm decreases and the NADH absorption peak at 340 nm gradually disappears, with subsequent buildup of the absorbance at 290 nm (Fig. 4e, 1.5 U complex I and 3.1 U complex I), and then the band is shifted to longer wavelengths (from 290 to 305 nm) as the concentration of complex I is increased (Fig. 4e, 4.1 U complex I), which indicates that ubiquinone could be reduced to ubiquinol[29]. This absorption profile demonstrates that ubiquinone accepts two-electrons and two-protons from
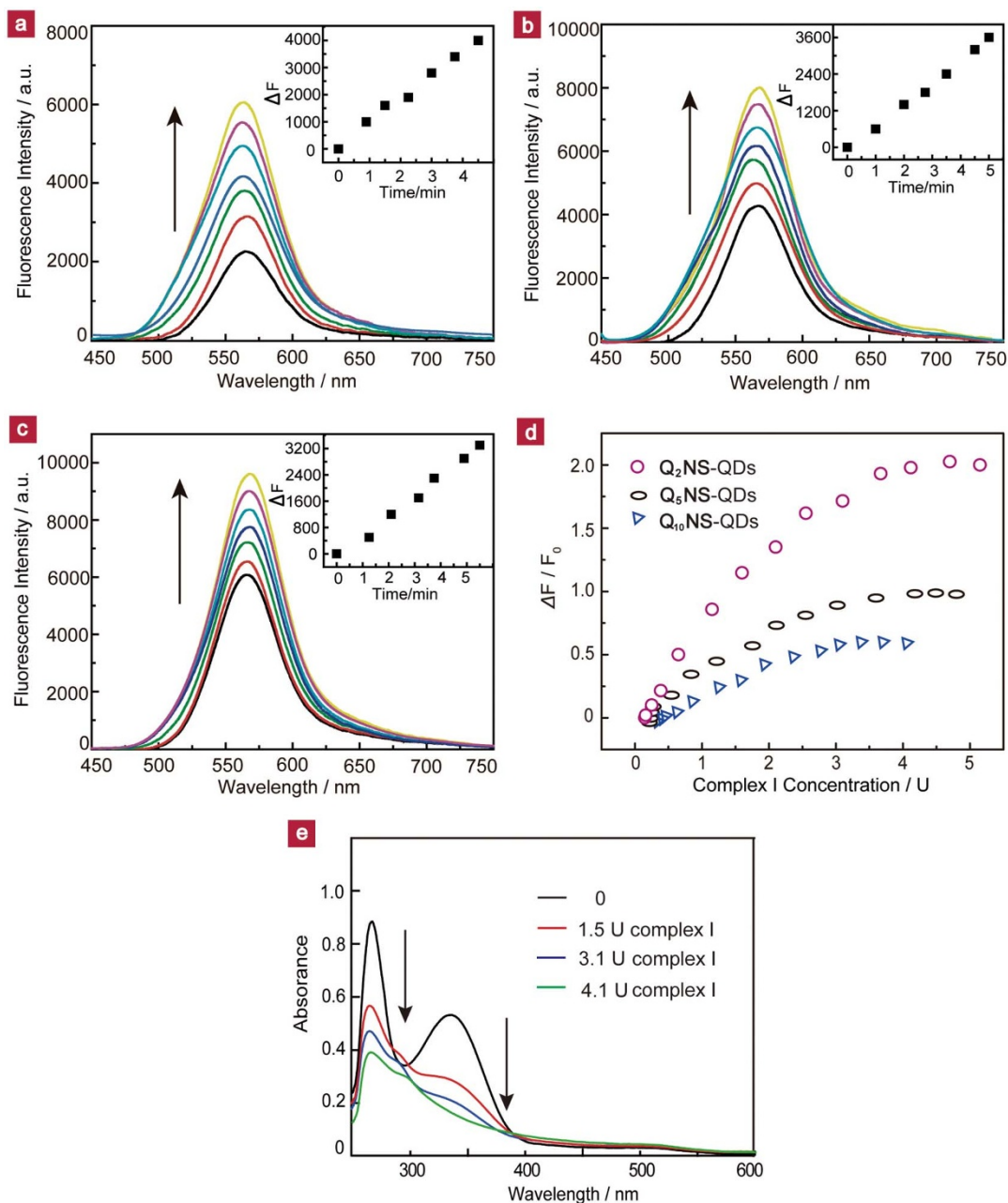
Figure 4 | Complex I sensing *in vitro*. (a–c), Time-dependent fluorescence changes upon the interaction of **Q₂NS** (a), **Q₅NS** (b) and **Q₁₀NS** (c) functionalised CdSe/ZnS QDs with complex I (4.9 U) in the presence of 10 mM NADH. The insets illustrate the increase of fluorescence (ΔF) as a function of incubation time. (d) Calibration curve corresponding to the fluorescence analysis of variable concentrations of complex I of **QₙNS**-QDs in the presence of NADH. (e) Absorption spectra changes observed upon addition of complex I to a deaerated PBS solution of **Q₅NS**-functionalised CdSe/ZnS QDs in the presence of 10 mM NADH. All measurements were performed in a 0.2 M deaerated PBS solution of pH 8.0.

NADH to convert to ubiquinol on the QDs' surface under biocatalysis of complex I to mimic the initial stage of respiration.

Discussion

The fluorescence enhancement and quenching of QD bioconjugates could be reversibly switched with the redox state of surface-capping ligands, between **QₙNS** and **HQₙNS**. Following photoexcitation of **QₙNS**-QD bioconjugates, QDs' CB electron is transferred to the lowest unoccupied molecular orbital (LUMO) of the ubiquinone acceptor and the electron is then shuttled back to the QDs' valence band (VB) through non-radiative pathways, releasing heat (Fig. 1c). Thus, ubiquinones exhibit surface-related trap states acting as fast non-radiative de-excitation routes for photoinduced electron carriers,

leading to fluorescence quenching[24]. It is worth noting that assembling **HQₙS** ligands on the CdSe/ZnS QDs produced a significant fluorescence enhancement. Here, the photoexcited **HQₙNS**-QD bioconjugates decay radiatively to the ground state because the **HQₙNS** ligands could act as poor electron acceptor/donors. This in turn will result in a recovery of high luminescence compared to unmodified QDs. Moreover, the ubiquinol also provides an efficient passivation of the surface trap states to overcome the potential surface defects, giving rise to a significantly enhanced fluorescence in such QD bioconjugates. As can be shown in Figure 1c, the bandgap of surface-capping ligand ubiquinol is larger than that of CdSe/ZnS QDs and the hole trapping is negligible. Upon excitation, the resulting electrons and holes are confined in the regions of the ubiquinol functionalised CdSe/ZnS QDs and thereby enhance the fluorescence. In

addition, the fluorescence efficiency and stability of HQ_nNS-QD bioconjugates against photo-oxidation has shown significant improvement due to the antioxidation effect of ubiquinol. Therefore, there is the remarkable fluorescence enhancement for HQ_nNS-functionalised QDs.

We show fluorescence change efficiency to be dependent on alkyl spacer, as more pronounced change was observed for shorter spacer in Figure 2a–c. This arises as decreasing spacer distance allows for faster electron-transfer rate, enhancing the ability of electron transfer between photoexcited QDs and Q_nNS. To confirm that the spacer-dependent Q_nNS ligands in the QD bioconjugates determine the magnitude of electron-transfer ability and concomitant QDs' fluorescence difference, we exploited the electrochemistry of Q_nNS-QDs in PBS buffer. Only a single pair of oxidation/reduction peaks were observed from Q_nNS-QDs, the voltammetric responses range from reversible for Q_2NS-QDs to irreversible for Q_5NS-QDs and $Q_{10}NS$-QDs based on the peak to peak separation (ΔE_p) as shown in Figure 2d. This is a typical cyclic voltammogram of surface-confined quinone monolayers measured in buffer where two-electron, two-proton transfer processes occur[30–32]. As the alkyl spacer increases, the ΔE_p increases because the electron transfer from photoexcited QDs to the redox active ubiquinone moiety is forced to proceed at a larger distance, slowing the overall electron-transfer rate and redox kinetics. Moreover, we retain the same electrochemistry as free Q_nNS (unmodified to QDs) in PBS buffer. As observed, the peak potentials of free Q_nNS are slightly different and redox shape is almost identical. As the spacer length increases from Q_2NS to $Q_{10}NS$, their cyclic voltammograms undergo a consistent shift in anodic and cathodic peak to lower potential (see Fig. S3, Supplementary Information). The ΔE_p of Q_2NS-QDs, Q_5NS-QDs and $Q_{10}NS$-QDs are 33, 107 and 223 mV, respectively, while the ΔE_p value of free Q_2NS, Q_5NS and $Q_{10}NS$ were typically larger. The great differences of voltammetric response between free Q_nNS and Q_nNS-QDs under the same conditions indicate that electron-transfer ability is affected when Q_nNS is covalently bound to the QDs' surface. We show fluorescence change efficiency to be dependent on alkyl spacer, as decreasing spacer distance enhances the ability of electron-transfer between the photoexcited QDs and the Q_nNS.

It is important to note that the capping layer of Q_nNS on QDs can be reduced to the ubiquinol form and effectively produce the high fluorescence of HQ_nNS-modified QDs, even at low concentrations of complex I. Similar to what occurred in initial stage of natural respiratory chain, changes in absorption were noted under our constructed QDs system as ubiquinol formed during the incubation process. This is also consistent with the electrochemical reduction of the ubiquinone capping layer to the reduced state ubiquinol that yields QDs of enhanced fluorescence. Exploiting these results suggest that Q_nNS-QDs could be a biocompatible fluorescence biosensor for tracking of complex I. Our goal was to establish a model to monitor intracellular complex I level using human neuroblastoma SH-SY5Y cells labelled with Q_nNS-QDs. The mitochondrial-specific neurotoxin such as rotenone was shown to inhibit complex I in the electron-transfer chain of mitochondria and induce PD, and PD patients were found to have the reduced levels of complex I activity[33]. Several lines of evidence suggest that complex I deficiency of mitochondria could represent an early critical evaluation in the pathogenesis of sporadic PD (Fig. 1f)[5–8]. We selected Q_2NS-CdSe/ZnS QDs with the best detection limit for complex I to investigate whether there are significant differences in fluorescence imaging of QDs as a function of complex I. Complex I levels decrease in human SH-SY5Y cells after 24 hr of exposure to 100 nM (Damage I), 500 nM (Damage II) and 1 µM (Damage III) rotenone. In Figure 5, Q_2NS-CdSe/ZnS QDs label SH-SY5Y living cells with different complex I levels: with no-damage (Normal), QDs' fluorescence is striking bright at cellular region. As the cell becomes more damaged (Damage I and Damage II), QD labelling produces a moderate fluorescence. With
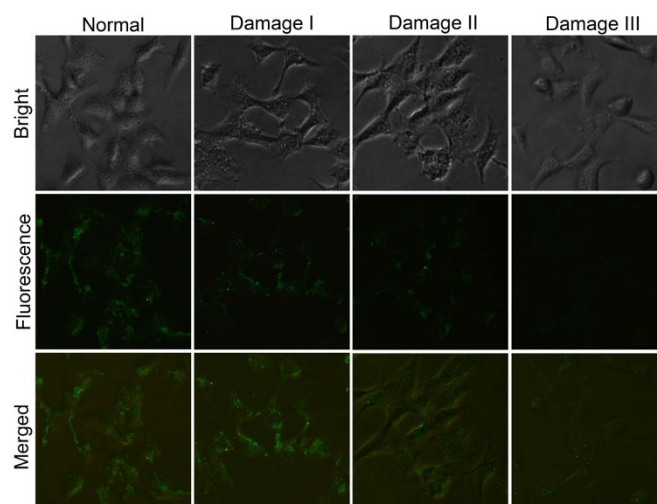

Figure 5 | Intracellular complex I level sensing. Bright field image and fluorescent micrographs collected from human neuroblastoma SH-SY5Y cells with 550-nm-emitting Q_2NS-functionalised QDs. Complex I deficient level increased in human SH-SY5Y cells after 24 hr of exposure to 100 nM (Damage I), 500 nM (Damage II) and 1 µM (Damage III) rotenone. A steady fluorescence decrease in Q_2NS-QDs label SH-SY5Y cell fluorescent micrographs as increase of complex I deficiency exhibits excellent concordance with *in vitro* result data. Merged images are shown in the bottom row.

the most-damaged cellular conditions (Damage III), QD labelling throughout the cell shows only faint fluorescence under identical conditions. A steady decrease in QDs' fluorescence correlated to complex I deficiency, whereas bright-field measurements clearly show that the cells are viable and overall cellular morphology appeared unperturbed during the process of these experiments (Fig. 5). The cell fluorescent micrographs exhibit excellent agreement with the *in vitro* data from Figure 4. These results suggest methods for our constructed Q_nNS-QDs system could trace complex I deficient levels in SH-SY5Y cells and have raised exciting possibilities in fluorescence biosensor targeting for PD diagnosis. Moreover, we also investigated the cytotoxicity of Q_2NS-QD labelled SH-SY5Y cells by the MTT assay. It is worthy to note that the cell viability after addition of Q_2NS-QDs was found to be above 80% at concentrations ranging from 3.75 to 200 µg·ml^{-1} for different rotenone damaged SH-SY5Y cells (see Fig. S4, Supplementary Information). Thus, Q_2NS modified CdSe/ZnS QDs are suitable for use in some potential biomedical applications.

In summary, we report the development of a novel biosensing approach using surface-attached CdSe/ZnS QDs exploiting three ubiquinone-terminated disulphides (Q_nNS). The fluorescence enhancement of reduced HQ_nNS-modified QDs and quenching of oxidized Q_nNS-modified QDs could be reversibly tuned with the transformation between Q_nNS and HQ_nNS state. In the presence of NADH and complex I, the surface attached layer Q_nNS-QDs was reduced to HQ_nNS by proton coupled electron-transfer from NADH to ubiquinone, which in turn enabled us to probe the complex I level by modulating the QDs' fluorescence intensity. Importantly, the utility of the system is demonstrated by monitoring the fluorescence change to trace complex I levels in human neuroblastoma SH-SY5Y cells. Our results demonstrate that the Q_nNS-QDs biosensor could be useful for early detection of PD and monitoring disease progression. We believe that our biosensing approach is a significant step forward toward molecular diagnosis of PD.

Methods

Fluorescence spectra of functionalised CdSe/ZnS QDs. 550 nm-emitting CdSe/ZnS core-shell QDs were hydrophilic with carboxylic acid ligands. 1 mM Q_nNS (oxidized

form, ubiquinone) and **HQ$_n$NS** (reduced form, ubiquinol) stock solutions were resolubilised in Millipore H$_2$O/dimethylsulphoxide (90:10) and self-assembled to CdSe/ZnS QDs in 0.2 M PBS at pH 8.0 for 30 min (for detailed procedures, see Supplementary Information). The **Q$_n$NS** and **HQ$_n$NS**-functionalised QDs stock solutions (0.2 μM) were purged with N$_2$ for 5 min before fluorescence analysis.

Cell Culture, cellular imaging and cytotoxicity. SH-SY5Y neuroblastoma cells were grown in Dulbecco's Modified Eagle Medium (DMEM, Gibco BRL, Paisley, UK) supplemented with 10% fetal bovine serum (Gibco BRL), 100 U·ml^{-1} penicillin and 100 μg·ml^{-1} streptomycin. Cells were maintained in a humidified 5% CO$_2$ atmosphere at 37°C. Environmental toxins such as the complex I inhibitor rotenone induce selective death of dopaminergic neurons through inhibition of the electron-transfer chain complex I activity. Rotenone was added directly to the media at appropriate concentrations. Complex I deficiency levels increased in human SH-SY5Y cells after 24 hr of exposure to 100 nM, 500 nM and 1 μM rotenone. Under these conditions, cell viability decreased by about 13%, 15% and 18% after 24 hr, respectively. SH-SY5Y cells with different complex I levels were plated into a 24-well culture plate (200-300 cells/well), and allowed to adhere for 10 hr before treatment. Culture medium containing 200 μg·ml^{-1} Q$_n$NS-functionalised CdSe/ZnS QDs were added and incubated for 10 hr. Next, the growth medium was removed, and the cells were fixed with 4% methanal solution at room temperature for 20 min, followed by washing three times with PBS solution. The cover glass was then mounted on a microscopic glass slide and was studied under a microscope. The images were taken by using an inverted fluorescence scanning microscope with an objective lens (×60). All background parameters (the laser intensity, exposure time, objective lens) were kept constant when the different fluorescence images were captured.

The cytotoxicity assays were performed by the MTT (3-(4,5-dimethylthiazol-2-yl)-2,5-diphenyltetrazolium bromide) assay. SH-SY5Y cells were placed in 96-well culture plates (10^4 cells/well), and allowed to attach for 24 hr before treatment. The cells were treated with **Q$_n$NS**-functionalised CdSe/ZnS QDs ranging from 3.75 to 200 μg·ml^{-1}. The cell viability was evaluated by the MTT assay for different rotenone damaged SH-SY5Y cells after 24 hr treatment. The optical density in control and sample-treated wells was measured in an automated microplate reader (Multiskan Ex, Lab systems, Finland) at a test wavelength of 470 nm. The cytotoxicity of modified QDs was expressed as IC$_{50}$ (concentration of 50% cytotoxicity, which was extrapolated from linear regression analysis of the experimental data).

1. Siderowf, A. & Stern, M. Update on Parkinson disease. *Ann. Intern. Med.* **138**, 651–658 (2003).
2. Dawson, T. M. & Dawson, V. L. Neuroprotective and neurorestorative strategies for Parkinson's disease. *Nat. Neurosci.* **5**, 1058–1061 (2002).
3. Jellinger, K. A. Neuropathological spectrum of synucleinopathies. *Mov. Disord.* **18**, S2–S12 (2003).
4. Litvan, I. *et al.* The etiopathogenesis of Parkinson disease and suggestions for future research. Part I. *J. Neuropathol. Exp. Neurol.* **66**, 251–257 (2007).
5. Shi, M. *et al.* Cerebrospinal fluid biomarkers for Parkinson disease diagnosis and progression. *Ann. Neurol.* **69**, 570–580 (2011).
6. Dawson, T. M. & Dawson, V. L. Molecular pathways of neurodegeneration in Parkinson's disease. *Science* **302**, 819–822 (2003).
7. Valente, E. M. *et al.* Hereditary early-onset Parkinson's diseasecaused by mutations in PINK1. *Science* **304**, 1158–1160 (2004).
8. Betarbet, R. *et al.* Chronic systemic pesticide exposure reproduces features of Parkinson's disease. *Nat. Neurosci.* **3**, 1301–1306 (2000).
9. Sazanov, L. A. & Hinchliffe, P. Structure of the hydrophilic domain of respiratory complex I from Thermus thermophilus. *Science* **311**, 1430–1436 (2006).
10. Jeya, M., Moon, H. J., Lee, J. L., Kim, I. W. & Lee, J. K. Current state of coenzyme Q$_{10}$ production and its applications. *Appl. Microbiol. Biot.* **85**, 1653–1663 (2010).
11. Matthews, R. T., Yang, L., Browne, S., Baik, M. & Beal, M. F. Coenzyme Q$_{10}$ administration increases brain mitochondrial concentrations and exerts neuroprotective effects. *Proc. Natl. Acad. Sci. U. S. A.* **95**, 8892–8897 (1998).
12. Do, T. Q., Schultz, J. R. & Clarke, C. F. Enhanced sensitivity of ubiquinone-deficient mutants of Saccharomyces cerevisiae to products of autoxidized polyunsaturated fatty acids. *Proc. Natl. Acad. Sci. U. S. A.* **93**, 7534–7539 (1996).
13. Michalet, X. *et al.* Quantum dots for live cells, in vivo imaging, and diagnostics. *Science* **307**, 538–544 (2005).
14. Melinger, J. S., Blanco-Canosa, J. B., Dawson, P. E. & Mattoussi, H. Quantum-dot/dopamine bioconjugates function as redox coupled assemblies for *in vitro* and intracellular pH sensing. *Nat. Mater.* **9**, 676–684 (2010).
15. Gao, X., Cui, Y., Levenson, R. M., Chung, L. W. K. & Nie, S. *In vivo* cancer targeting and imaging with semiconductor quantum dots. *Nat. Biotechnol.* **22**, 969–976 (2004).
16. Gao, J. *et al.* In vivo tumor-targeted fluorescence imaging using near-infrared non-cadmium quantum dots. *Bioconjugate Chem.* **21**, 604–609 (2010).
17. Gill, R., Zayats, M. & Willner, I. Semiconductor quantum dots for bioanalysis. *Angew. Chem. Int. Ed.* **47**, 7602–7625 (2008).
18. Medintz, I. L., Tetsuouyeda, H., Goldman, E. R. & Mattoussi, H. Quantum dot bioconjugates for imaging, labelling and sensing. *Nat. Mater.* **4**, 435–446 (2005).
19. Chan, W. C. W. & Nie, S. Quantum dot bioconjugates for ultrasensitive nonisotopic detection. *Science* **281**, 2016–2018 (1998).
20. Medintz, I. L., Tetsuouyeda, H., Goldman, E. R. & Mattoussi, H. Quantum dot bioconjugates for imaging, labelling and sensing. *Nat. Mater.* **4**, 435–446 (2005).
21. Clarke, S. J. *et al.* Photophysics of dopamine-modified quantum dots and effects on biological systems. *Nat. Mater.* **5**, 409–417 (2006).
22. Cooper, D. R. *et al.* Photoenhancement of lifetimes in CdSe/ZnS and CdTe quantum dot-dopamine conjugates. *Phys. Chem. Chem. Phys.* **11**, 4298–4310 (2009).
23. Cooper, D. R., Dimitrijevic, N. M. & Nadeau, J. L. Photosensitization of CdSe/ZnS QDs and reliability of assays for reactive oxygen species production. *Nanoscale* **2**, 114–121 (2010).
24. Qin, L. X. *et al.* Coenzyme Q functionalised CdTe/ZnS quantum dots for reactive oxygen species (ROS) imaging. *Chem.-Eur. J.* **19**, 5262–5271 (2011).
25. Li, D.-W. *et al.* CdSe/ZnS quantum dot-Cytochrome c bioconjugates for selective intracellular O$_2$·$^{-}$ sensing. *Chem. Commun.* **47**, 8539–8541 (2011).
26. Chan, T. R., Hilgraf, R., Sharpless, K. B. & Fokin, V. V. Polytriazoles as copper (I)-stabilizing ligands in catalysis. *Org. Lett.* **6**, 2853–2855 (2004).
27. Shen, R. *et al.* Multifunctional conjugates to prepare nucleolar-targeting CdS quantum dots. *J. Am. Chem. Soc.* **132**, 8627–8634 (2010).
28. Hirst, J. Towards the molecular mechanism of respiratory complex I. *Biochem. J.* **425**, 327–339 (2010).
29. Ma, W. *et al.* In situ spectroeletrochemistry and cytotoxic activities of natural ubiquinone analogues. *Tetrahedron* **67**, 5990–6000 (2011).
30. Costentin, C. Electrochemical approach to the mechanistic study of proton-coupled electron transfer. *Chem. Rev.* **108**, 2145–2179 (2008).
31. Hong, H. G. & Park, W. Electrochemical characteristics of hydroquinone-terminated self-assembled monolayers on gold. *Langmuir* **17**, 2485–2492 (2001).
32. Abhayawardhana, A. D. & Sutherland, T. C. Heterogeneous proton-coupled electron-transfer of a hydroxy-anthraquinone self-assembled monolayer. *J. Electroanal. Chem.* **653**, 50–55 (2011).
33. Sherer, T. B., Betarbet, R., Kim, J. H. & Greenamyre, J. T. Selective microglial activation in the rat rotenone model of Parkinson's disease. *Neurosci. Lett.* **341**, 87–90 (2003).

Author contributions

W.M. and L.-X.Q. contributed equally to this work. W. M. synthesized **Q$_n$NS** compounds. W.M. and L.-X.Q. designed and performed all the experiments, and wrote the manuscript. F.-T.L. and J.W. grew cell cultures and assisted with cellular experiments. G.Z. drew and summarized the figures. Y.-T.L., Z.G.P. and T.D.J. finalized the preparation of the manuscript. Y.-T.L. designed and managed the project. All the authors discuss the results and commented on the manuscript.

Additional information

How to cite this article: Ma, W. *et al.* Ubiquinone-quantum dot bioconjugates for *in vitro* and intracellular complex I sensing. *Sci. Rep.* **3**, 1537; DOI:10.1038/srep01537 (2013).

CORRIGENDUM: Ubiquinone-quantum dot bioconjugates for *in vitro* and intracellular complex I sensing

Wei Ma, Li-Xia Qin, Feng-Tao Liu, Zhen Gu, Jian Wang, Zhi Gang Pan, Tony D. James & Yi-Tao Long

The authors have noticed that Figure 1 was published incorrectly in the original version of this Article. The correct Figure 1 appears below.
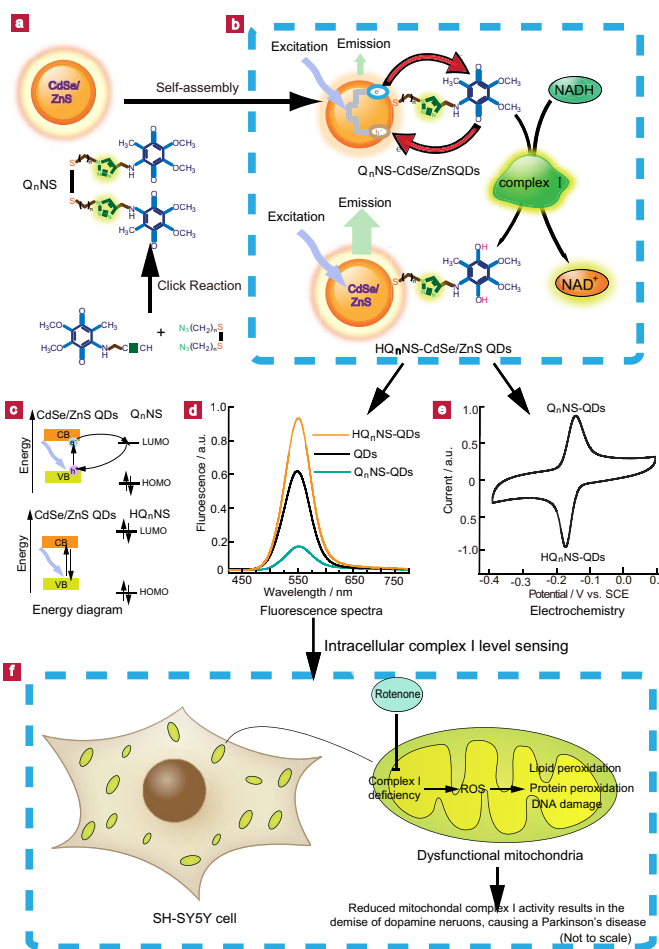

Figure 1 | Schematic of ubiquinone-CdSe/ZnS QDs as redox fluorescence biosensor for Parkinson's disease diagnosis. (a), Ubiquinone-terminated disulphides ($\mathbf{Q_nNS}$) synthesis and self-assembly of $\mathbf{Q_nNS}$ on to CdSe/ZnS QDs. (b), Conceptual visualisation of $\mathbf{Q_nNS}$-QDs as complex I sensor *in vitro*. Under oxidized state ($\mathbf{Q_nNS}$), ubiquinone functions as a favorable electron acceptor, this results in effective QDs' fluorescence quenching. Addition of complex I to $\mathbf{Q_nNS}$-QDs solution in the presence of NADH, ubiquinone coupled electron transfer and proton translocation from NADH, producing reduced ubiquinol ($\mathbf{HQ_nNS}$) form on the surface of QDs to mimic the initial stages of the respiratory chain. Ubiquinol when in close proximity to the QDs produces fluorescence enhancement. (c), Energetic diagram of the QDs bioconjugates between QDs and $\mathbf{Q_nNS/HQ_nNS}$. (d), Fluorescence spectra of ubiquinone/ubiquinol- functionalised CdSe/ZnS QDs. (e), Cyclic voltammetry of $\mathbf{Q_nNS}$-CdSe/ZnS QDs. (f), Visualisation of $\mathbf{Q_nNS}$-CdSe/ZnS QDs as an intracellular complex I sensor. The mitochondrial-specific neurotoxin, rotenone, inhibits complex I and leads to Parkinson's-like pathogenesis. Parkinson's disease is characterised by impaired activity of complex I in mitochondria.